Pressure and temperature diagram of C60 from atomistic simulations

Karim Hakim, Romain Dupuis, Christophe Bichara, R.-J.-M. Pellenq

Pressure and Temperature Diagram of C_{60} from Atomistic Simulations

Karim Hakim[1], Romain Dupuis[2], Christophe Bichara[1], Roland. J.-M. Pellenq[3*]

1 CINaM, CNRS and Aix-Marseille Univ, Campus de Luminy, 13288 Marseille, cedex 09, France

2 LMGC, Univ. Montpellier, CNRS, Montpellier, France

3 IEM, CNRS and University of Montpellier, 300 Av. du Professeur Jeanbrau, 34090 Montpellier, France

* Corresponding author: roland.pellenq@cnrs.fr

Abstract

Although widely studied experimentally in the 1990s, the structure and properties of low dimensional or high-pressure phases of fullerenes have recently been re-examined. Remarkably, recent experiments have shown that transparent, nearly pure amorphous sp^3-bonded carbon phases can be obtained by heating a C_{60} molecular crystal at high pressure. With the additional aim of testing the ability of three classical carbon potentials (REBO, EDIP and ReaxFF) to reproduce these results, we investigate the details of the structural transformations undergone by fullerene crystals over a wide range of pressures and temperatures. All the potentials tested show that the initial polymerization of fullerenes is accompanied by negative thermal expansion, albeit in slightly different ranges. However, more significant differences in structural and mechanical properties are observed in the amorphous phases, in particular the sp^3 carbon fraction and the existence of layered amorphous carbon. Overall, these results indicate to which extent classical reactive potentials can be used to explore phase transitions over a wide range of pressures and temperatures.

Introduction

Since their discovery in 1985 by Kroto *et al.* [1], C_{60} fullerenes have raised a strong interest among researchers across various fields due to their distinctive properties and potential applications. They have been used in many fields, from electrocatalysis to electrochemistry, optics, and mechanical properties, [2], [3], [4], [5]. C_{60} is a carbon nano-sphere with a diameter of 0.7 nm whose 60 carbon atoms are three-fold coordinated with their bonds forming 20 hexagons and 12 pentagons. In condensed state, C_{60} can exist as a molecular crystal or glassy phases. Interestingly enough, C60 liquid phase has never been observed. The face-centered cubic (FCC) phase of C_{60} is the most commonly observed and, in addition to being the most stable crystalline state, its distinctive electronic and optical properties hold promise for applications in fields such as electronics and photovoltaics [6]. Nevertheless, despite extensive research into the FCC phase of C_{60}, much remains to be discovered about its behavior under high P,T conditions. Under such pressures, the fullerene may collapse and the reversibility of the transformation has been questioned. The first questions about reversibility and the fullerene/amorphous phase change were raised by Duclos *et al.* [7]. With the experimental methods available in the 90's, researchers were able to set the reversibility point between 17 and 25 GPa [8]. Two years later, using a diamond anvil cell the transition pressure has been measured at 18 GPa and the observed scratches on the anvils suggested that the amorphous material created was harder than diamond [9]. The Raman spectrum measured at ambient on the amorphous carbon obtained corresponds neither to that of diamond nor to that of graphite, suggesting the existence of a new carbon phase. Prior to this, theoretical calculations were performed to compute the bulk modulus of C_{60} crystals and it was thought that a C60 material as strong as diamond or even stronger might be found [10].

Since then, it has been demonstrated that high-pressure and high-temperature conditions have a significant impact on the crystalline structure of C_{60}, giving rise to new phases and unexpected phenomena. During the transition from a molecular phase to a polymerized phase, covalent bonds are

formed between the fullerenes, and amorphous, layered or diamond-like phases can be obtained [11], [12]. Although the existence of a polymerization of C_{60} molecules and the formation of an ultra-hard solid at high pressure and temperature were demonstrated in the 1990's, the study of these phenomena is still active. Sabirov *et al.* have studied the structure and connections of fullerenes forming linear and zigzag nanoaggregates and the fusion of two C_{60}s into C_{120} [13], while bidimensional networks created by polymerization of C_{60} were studied by Meirzadeh *et al.* [14]. It should be noted that a negative thermal expansion for temperatures in the 300 K - 800 K range was observed at 9.5 GPa in 1995 [12], but little mentioned since. Phases of C_{60} chains, 2D and 3D crystals at various pressures and temperatures have been identified [6], [15], [16]. Recently, simulations using a neural network potential and stochastic surface walking showed that the electronic properties of the initially C_{60} crystals are modified under pressure. This suggests that novel carbon structures might be prepared in high pressure experiments on C_{60} [17]. At the same time, Shang *et al.* [18] have shown that it is possible to obtain an amorphous material with peak bulk modulus and maximum transparency as well as a maximum sp^3 fraction at 27 GPa and 1000 degrees Celsius.

The aim of this work is to use atomistic computer simulation techniques to study the successive transformations of cubic C_{60} crystals into various amorphous phases, from room temperature up to 60 GPa and 2000 K, in order to analyze their structure and calculate their mechanical properties in relation to this recent article. Tight-binding molecular dynamics simulations have shown that a shearing leads to an easier collapse of C_{60} at lower pressure [19]. In order to mimic the experiments [18] as closely as possible, we will employ purely compressive stress. Using reactive Molecular Dynamics computer simulations, this work also enables interatomic C-C potentials to be tested over a wide range of pressures and temperatures. C_{60} polymerization and negative thermal expansion are found using all potentials, albeit in slightly different pressure and temperature ranges, while greater differences in structural and mechanical properties are observed in the amorphous phases.

Methods

To investigate the system's response to varying pressures and temperatures, we conducted extensive simulations using NVT and NPT Molecular Dynamics (MD) employing the LAMMPS software package [20]. The NVT and NPT ensembles were simulated using Nose–Hoover thermostat and barostat [21]. Parameters of those were chosen for carbon materials following [22] for a timestep of 0.5ps. Our simulated system contained 32 C_{60} fullerene molecules, with temperature conditions spanning the range of 300 to 2000 K, and pressures ranging from 1 to 60 GPa. Prior to initiating the NPT ensemble simulations, we employed an initial equilibration step conducted in the NVT ensemble. Following the equilibration phase, we performed the NPT ensemble simulations over 1.5 10^9 steps, spanning 750 ns. In this work, we have used three Bond Order potentials (BO): the Reactive Empirical Bond Order (REBO), the Environment-Dependent Interatomic Potential (EDIP) and the Reactive force-field (ReaxFF). BO potentials are potentials that analytically calculate the binding energy between atoms as a function of their atomic environment, such as the number of neighbors, bond lengths and bond angles. They use analytical functions that describe bond-forming and bond-breaking and include 3-body contributions. The REBO potential considers Van der Waals interactions and a torsion (4-body) term [17]. The EDIP potential adds two terms of bond order, a two-body and a three-body term. It also considers dihedral rotation and π-repulsion, which enables better results to be obtained on layered structures, which are often due to the interlayers π-repulsion between the sp^2 atoms in the specific case of graphite [23], [24]. The ReaxFF potential uses distance-dependent bond order functions. It considers up to 14 different energy terms and allows continuous bond creation and destruction throughout the simulation [25]. Rebo was performed for 55 ns and Reax for 2 ns because of the slowness of the potential.

Results and discussion

The following results (Figures 1 – 5) were obtained with the EDIP interatomic C-C potential. When necessary, we provide comparisons with results obtained with the REBO and ReaxFF force fields, as in Supplementary Material (SM) Figure S1. Figure 1 offers insights from numerical experiments exploring the behavior of C_{60} fullerene molecules starting from a FCC crystal, under a constant pressure set at 20 GPa and at different temperatures. Figure 1a obtained at 300 K, shows the molecular FCC crystal, wherein individual fullerene balls remain discernible, with no chemical bonding between them. This aligns with prior research findings on fullerenes under low-temperature and low-pressure conditions [6], [11], [26], [27].

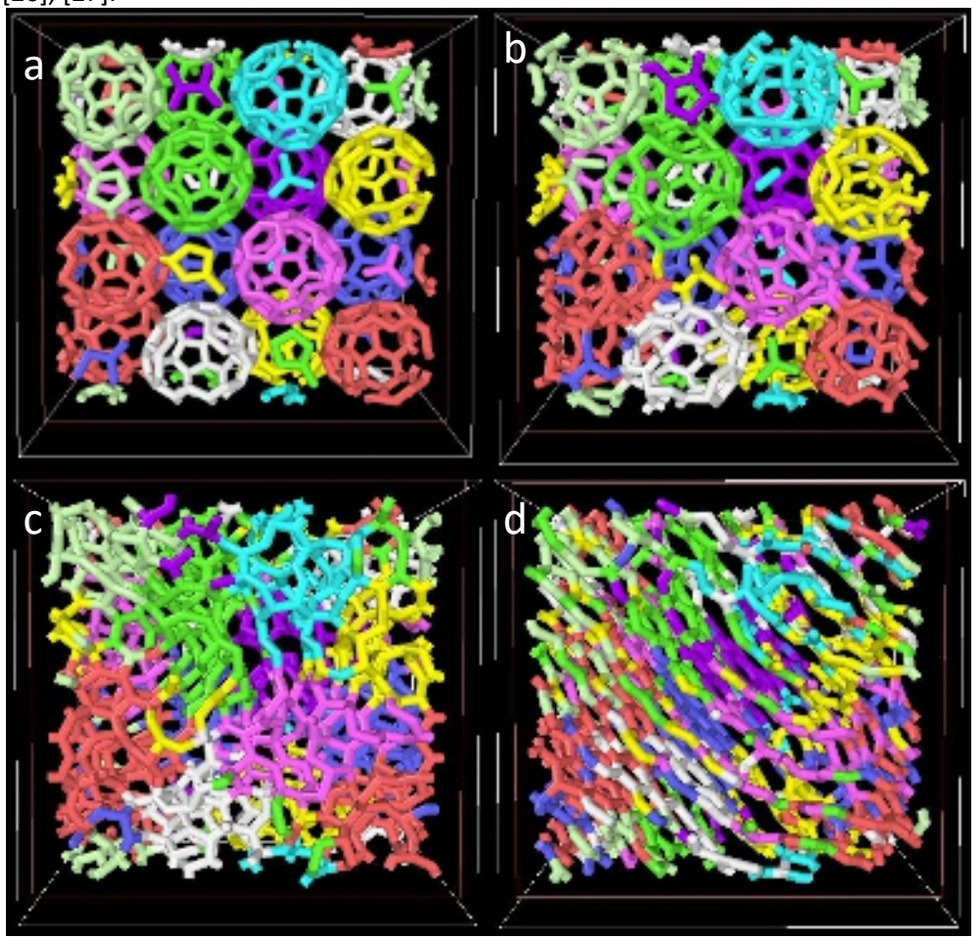

Figure 1*: Evolution of the structure at different temperatures, (a) 300 K, (b) 1000 K, (c) 1500 K and (d) 2000 K for at 20 GPa, obtained with the EDIP potential). The color code showing the atoms belonging to each initial C_{60} is kept throughout the different images, indicating a growing degree of intermixing with increasing temperature.*

In contrast, Figure 1b shows fullerene polymerization at 1000 K, resulting in the formation of covalent bonds between the fullerene molecules. This polymerization process has been previously observed and is thought to arise from pressure-induced volume reduction and reduced molecular mobility by hindering C_{60} rotation[6], [27], [28]. The polymerization process is characterized by an inter-fullerene distance close to 2.2 Å (see the pair C-C distribution function in Figure 4a). This agrees with the recent X-ray experimental data of Shang *et al.*[18]. It is worth noting that REBO and EDIP interatomic C-C potentials have a chemical bonding cut-off distance set at 2.0 and 2.2 Å respectively. The cut off distance is not so simply defined in ReaxFF [29] , but behaves as a smoother damping function acting up to 2.6 Å. Therefore, a question arises concerning the meaning of this peculiar 2.2 Å distance as seen in the simulation results. Experimentally, the key feature is a transition from a molecular crystal (with weak dispersion interaction between C_{60} molecules) to a chemically bonded set of fullerenes, reported

metallic [27], [30] . The nature of this elongated C-C bond remains to be clarified and this point is thoroughly discussed below.

Figure 1c (at 1500 K), reveals that the fullerenes have undergone a collapse process, towards an amorphous carbon phase. Notably, the amorphous carbon phase comprises pentagons and hexagons, which are remains of the initial fullerene molecular configuration. This collapse mechanism takes place in a wide range of pressures (10 – 50 GPa) at 1500 K. Furthermore, it's worth noting that the threshold temperature for amorphous carbon formation decreases with increasing pressure. Consequently, at higher pressures, amorphous carbon can be obtained at a lower temperature of 800 K.

In Figure 1d (at 2000K), we observed a recurrent phase change phenomenon: the initially amorphous and isotropic carbon material transforms into a layered structure consistent with a graphitization process. This alignment leads to the formation of almost parallel carbon layers exhibiting some structural patterns, including pentagons, hexagons, and heptagons. This graphitization transition takes place in a large pressure range, beginning at 10 GPa and persisting up to 40 GPa at temperatures of 2000K and beyond. Note that for pressures larger than 40 GPa no graphitization transition is observed. The amorphous carbon phase is found to have a very high bulk modulus, due to its lack of dislocations as shown in Figure 6b, in agreement with the simulation results of Zhao *et al.* [31]. These latter simulations used a different potential (GAP20), and uniaxial compression. However, we find molecular, polymerized, and amorphous phases in the same P,T domains. The different compression methods might explain why, using EDIP, we observed a layered phase which is by essence anisotropic, at lower temperature and up to higher pressure. The bulk moduli are in the same range (slightly below 1000 GPa), while our fraction of sp^3 carbon, which strongly depends on the potential used, is somewhat lower than in [31].

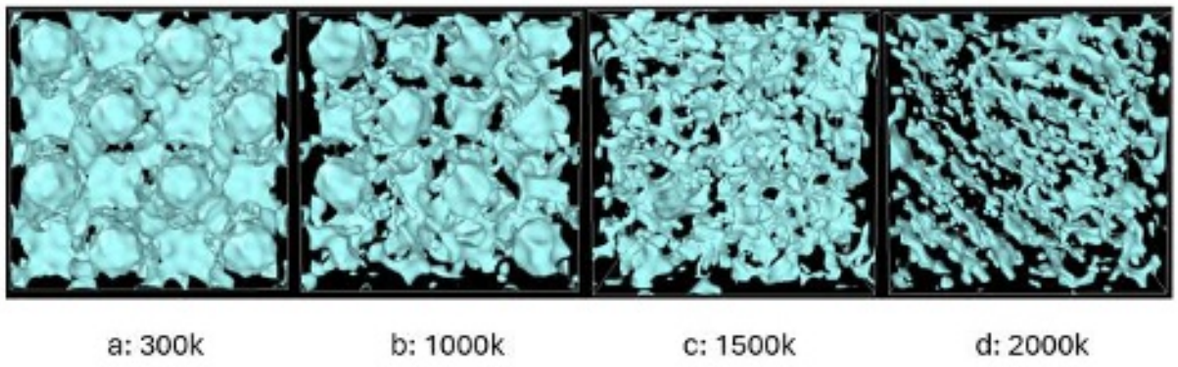

Figure 2*: Representation of the voids (in blue) for the different systems at 20 GPa (a) at 300 K (molecular system), (b) 1000 K (polymerized system), (c) 1500 K (amorphous system) and (d) 2000 K (layered system), obtained with the EDIP potential.*

To provide an alternative visualization, we show in Figure 2 the interstitial voids in the different phases shown in Figure 1. For the molecular system (Figure 2a, 20 GPa and 300K), the fullerene molecules maintain a non-contact configuration, with voids enveloping the blue spheres: fullerene crystal remains stable, exhibiting minimal deformation under the influence of pressure and temperature. Figure 2b, (20 GPa, 1000K), reveals a departure from molecular stability: fullerene molecules become deformed, which translates in a global decrease of the void fraction that characterizes the polymerization process. Figure 2c unfolds the collapsing process towards amorphous carbons (20 GPa, 1500 K). Consequently, the void within the system becomes less prevalent, as carbon atoms occupy the entire available volume. Finally, in Figure 2d, we examine the system (20 GPa, 2000K) in which carbon atoms reorganize and adopt a layered configuration characterized by void in-between layers. However, additional voids persist elsewhere, emphasizing that the layers do not exist in complete independence and uniformity but are 3d connected [32]. All these results were obtained using the EDIP interatomic C-C potential. It is interesting to note that similar results are obtained with the REBO potential on the same P,T domains although we note a lower extent of graphitization. As for ReaxFF,

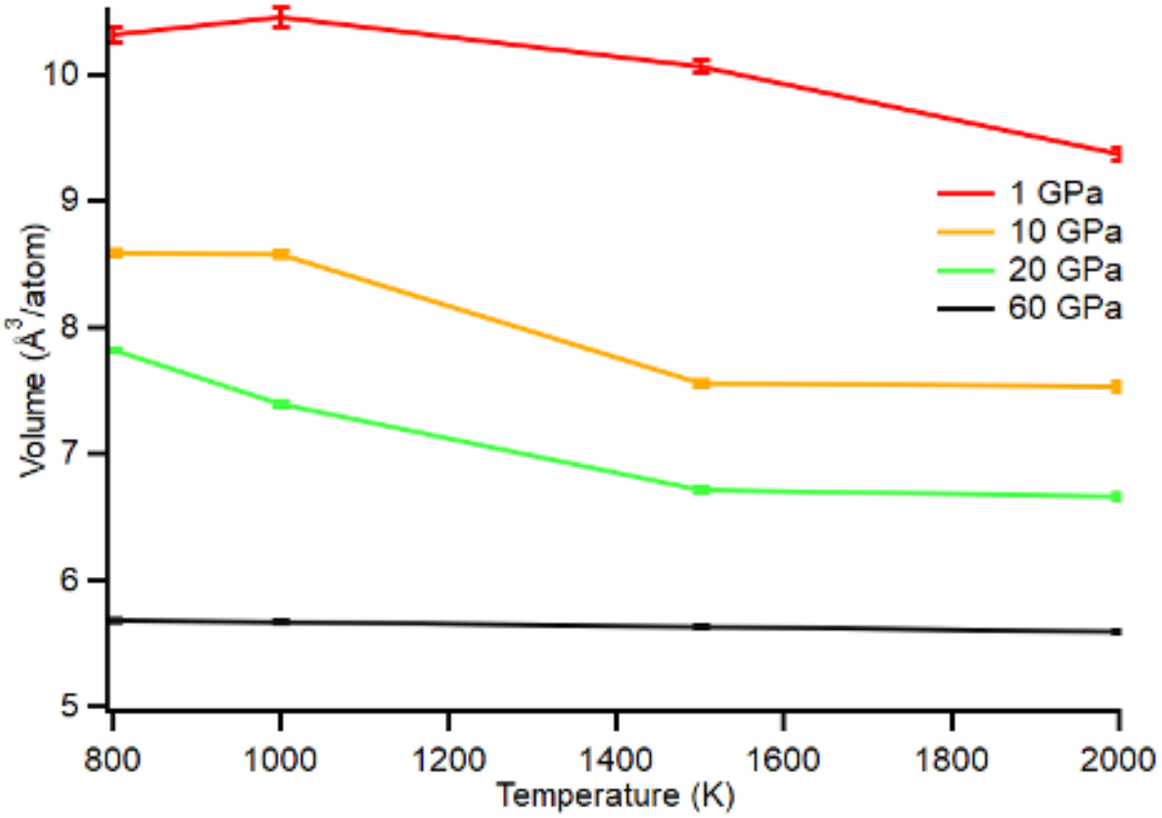

Figure 3: *Atomic volume as a function of temperature at pressures 1, 10, 20 and 60 GPa. At low to moderate pressures the volume decreases with increasing temperature, a signature of a negative thermal expansion caused by the polymerization of C_{60} molecules, as inter-C60 covalent bonds are formed. Standard deviations characterizing the fluctuations of the atomic volume are indicated by error bars. They become smaller as pressure increases.*

we find the molecular, polymerized and amorphous systems, but we did not observe any layered system. The initial phase transition from a molecular crystal to a polymerized crystal gives rise to a unusual negative thermal expansion (NTE) phenomenon: as temperature increases, there is a departure from the expected trend of volume expansion for molecular crystals; instead, a reduction in volume is observed (see Figure 3, 1 GPa to 60 GPa, spanning temperatures ranging from 800 K to 1500 K).At 1 GPa, the volume of the C_{60} fullerene crystal exhibits a temperature-dependent expansion between 800 K and 1000 K, followed by a contraction at 1500 K. As pressure increases to 10 GPa and 20 GPa, this negative thermal expansion (NTE) is observed at lower temperatures, and becomes negligible at 60 GPa. This volume contraction can be attributed to the polymerization of C_{60} molecules, involving the formation of C-C bonds between adjacent C_{60} carbons (see Figure 4a). By gradually lowering the temperature from 1000 K to 300 K starting from the polymerized phase (at constant pressure set to 20 GPa), no depolymerization is observed: the system shows densification as expected for most materials experiencing lower temperatures. Polymerization is therefore not temperature-reversible and polymerized C60 complies to usual behavior with temperature change. Conversely, at constant temperature (1000 K), as the pressure is reduced from 20 GPa to 1 GPa, the C60 molecules tend to separate and return to their molecular (initial) configuration hence leading to a global volume increase although some C60 molecules remain bounded (and deformed). Upon pression decrease, C60 polymerization is therefore (partially) reversible.

Interestingly, it has been a search for the liquid molecular phase of C60 that has never been observed experimentally. Costa et al [33] using a non-reactive potential did predict a full phase molecular C60 phase diagram in which the triple point was localized at 1975 K and 2 MPa and the critical point at

1930 K and 0.45 nm^{-3}, see SM Figure S6a). We then performed ReaxFF additional MD-NPT calculations in the following pressure-temperature conditions around the reported triple point starting from the fcc C60 crystal configurations: 1850 K, 1900 K and 1950 K under 0.1 MPa, 5 MPa and 10 MPa. Note that ReaxFF includes dispersion interaction under the form of a Lennard-Jones potential. In the 0.1-10 MPa pressure and 1850-1950K temperatures ranges, we obtained a density around 0.6 nm^{-3} that is actually very different from that predicted from Costa et al' phase diagram (see SM Figure S6b). Interestingly enough, the mildest considered conditions [1850 K under 0.1 MPa] actually correspond to a partial polymerized state and not to liquid C60 (see SM Figure S6c).

Increasing pressure indeed leads to a reduction in the inter-fullerene distance and a transition from a sp^2 to a sp^3 bonding state, for an increasingly larger number of carbon atoms, resulting in an augmented bulk modulus for the crystal structure (see Figure 6b).

Pair distribution functions, g(r), Figures 4a and 4b, were obtained at 1000 K and 2000 K, for pressures ranging from 1 to 60 GPa. The molecular crystalline state is characterized by a series of well-defined peaks in the g(r). As expected, first neighbor distances slightly shift downwards with increasing pressures. As already mentioned, the polymerization characteristic C-C distance is found at 2.20 Å. The presence of this distance which persists even in the disordered phases at larger pressure deserves further investigation.

SM Figure S1 displays the pair distribution functions g(r) obtained with REBO, EDIP and ReaxFF at 60 GPa and 800 K. Figure S2 shows the detailed contributions to g(r) [34] obtained by creating histograms of the first, second … neighbors around each atom and averaging over all relevant configurations. We note that the three first neighbor shells are well defined in all examples and clearly monomodal. The distribution of the 4th neighbor distance is bimodal with a large gap between the two peaks. Some C atoms have 3 neighbors only, while others are 4-fold coordinated, which can be seen as a characteristic feature of the

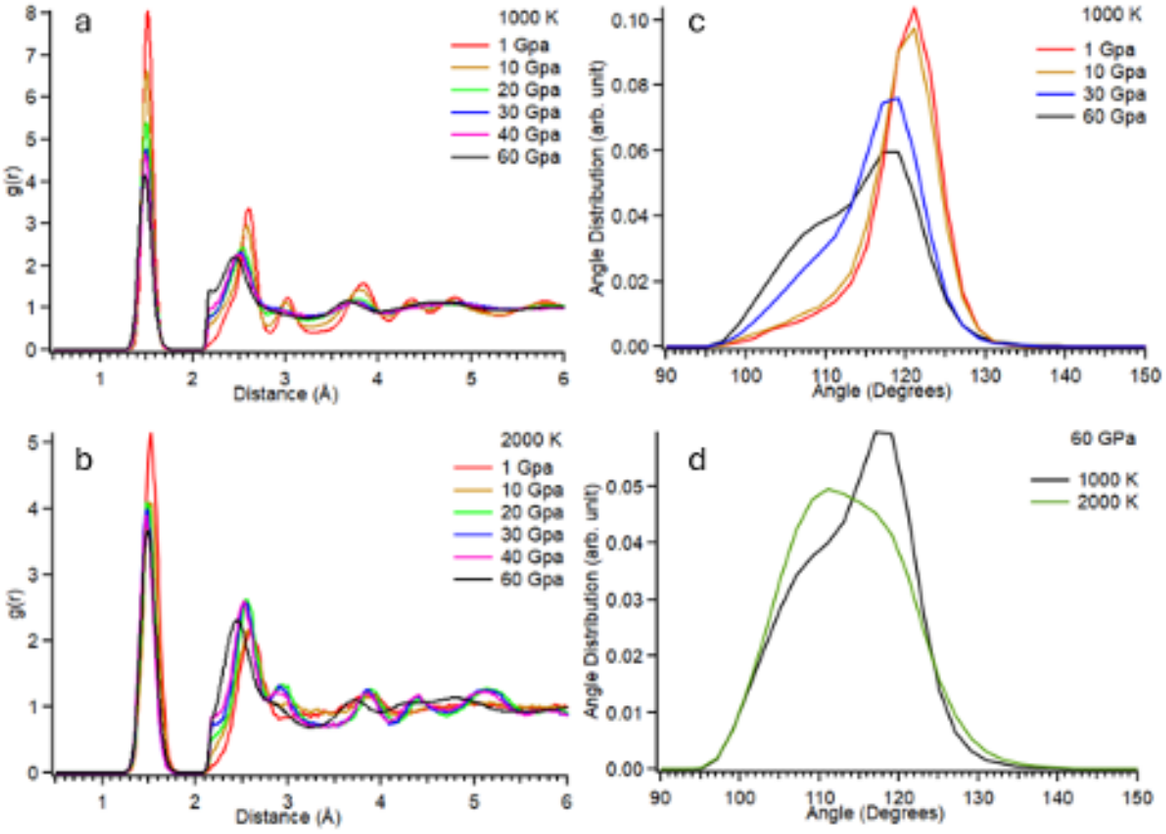

Figure 4: *Radial distribution function for 2 temperatures: (a) at 1000 K for 1, 10, 20, 30,40 and 60 GPa and (b) at 2000 K for the same pressure. (c) and (d) are the Bond Angle Distributions. Data obtained with the EDIP potential.*

gradual polymerization of neighboring fullerenes. We use this characteristic bimodal structure of the 4th neighbor distribution to evaluate the fraction of sp^3 bonded atoms by measuring the relative fraction of neighbors in each side of the distribution. We note however that the non-bonded (rightmost) part of the 4th peak sits just above the cut-off distances of REBO and EDIP potentials: the system gains energy by pushing some atoms outside the coordination shell, rather than paying the price of overcoming the energy barrier associated with the sp^2-sp^3 transition. In all cases a depletion of neighbors is observed in a range around 1.8 Å, depending on the potential, raising the question of its physical validity.

To understand why such a pronounced gap, with a g(r) equal to zero, is observed in our calculations, we investigate the transition from rhombohedral graphite to diamond with the three potentials used. As early as 1987, Fahy *et al.* [35] evaluated the barrier for the graphite to diamond transition at 0.32 eV/C (at a C-C distance of 2.0 Å). Figure S3 presents energy barriers for the transition from rhombohedral graphite to diamond, calculated using REBO, EDIP and ReaxFF on box sizes containing 192 carbon atoms. Such sizes were used to accommodate the different cutoff distances. DFT calculations were performed on the structures relaxed using ReaxFF, without further relaxations to keep things comparable. Density functional theory single-point calculations have been performed using the SIESTA code. GGA-PBE functionals have been used with a Trouillier-Martins pseudopotential. A double-Z polarisation basis set has been used and Grimme D2 corrections have been applied. The mesh cutoff is 300 Ry and the calculations have been performed at the G point only [35-38]. The heights of all energy barriers are comparable and quite large, explaining the deep gap in g(r). They are shifted and become wider as the cut-off distances increase, in line with the reference DFT calculations. Because of their short cut off distances REBO and EDIP enable fast calculations but produce unphysical small peaks at these distances. ReaxFF is smoother but significantly slower.

We note however that the experimental pair distribution functions measured by Shang *et al.* [18] does not display the pronounced dip seen in all three simulations. On the contrary, the structure factors S(q), calculated (Figure 5) on our atomic models compare more favorably with the experimental ones. A reason might be that Fourier transforming S(Q), that is the direct output of the experiment, into g(r) is hampered by the limited Q-range (15 $Å^{-1}$) of the data, resulting in cut-off ripples, in particular between the first and second peaks of g(r). The enhanced view of the large Q domain offered by the plot of Q(S(Q) – 1) shows that EDIP provides a better description of the local order than REBO, in which the large Q oscillations tend to become out of phase, and to a lesser extent ReaxFF (Figure 5). So, for the remaining of this paper, we focus on EDIP potential results. As a distinctive feature, the amorphous phases are characterized by the absence of the third peak found in the molecular crystal or polymerized curves (see Figure 4a). Conversely, we note that this particular peak is again present in the graphitized structure (see Figure 4b).

However, at 2000 K, polymerized or molecular systems cease to exist; only the disordered and layered structures remain in the entire pressure range. At 1 and 10 GPa, the pair distribution profiles resemble those of the previously observed amorphous systems. In the pressure range from 20 to 40 GPa, a layered system emerges, featuring a reemergence of a 3rd peak, previously absent during amorphization, merging with the 2nd peak. At 60 GPa, the system retains its amorphous character. The first peak of g(r) remains relatively consistent across these systems, albeit shifting further downwards with increasing pressure. A similar behavior is noted for the second peak. The overall process therefore indicates a pressure-induced 3D-ordered/disordered/2D-ordered transformation with signature in the medium-range distances at temperatures lower than 2000 K. This goes with changes in the sp^3 to sp^2 fraction.

A complementary method to analyze the structures involves the Bond Angle Distributions (BAD). In Figure 4c, we present the BAD of the same four structures as in Figure 1 at a constant temperature of 1000K and 1 GPa, 10 GPa, 30 GPa, 60 GPa. The curves for the 30 GPa and 60 GPa systems are shifted to the left, featuring not only a peak at 117 degrees but also a shoulder at 109 degrees, while the curves at 1 GPa and 10 GPa exhibit a single peak at 120 degrees. The presence of the peak at 120 and 117 degrees corresponds to the prevalence of sp^2 carbons, indicative of the molecular system state.

However, in the 30 GPa and 60 GPa systems, the shoulder at 109 degrees is compelling evidence of the formation of sp^3 carbons confirming the transformation of sp^2 to sp^3 as the C_{60} molecules draw closer together under increased pressure.

Figure 4d presents the BAD of the initially C_{60} fullerene crystal at a constant pressure of 60 GPa at 1000 K and 2000 K. Even though the system maintains its amorphous character at 60 GPa, a discernible change occurs in the peak position. Specifically, the peak shifts from 117 to 109 angle degrees, signifying a predominant transition towards sp^3 hybridization, even though traces of sp^2 bonding persist. The large range of pressure and temperature changes shows that the transition towards sp3 requires overcoming high energy barriers. This transformation underscores a crucial trend in the system's behavior: as pressure intensifies, the system retains its amorphous nature but exhibits an increased fraction of sp^3 hybridization (65%), aligning with experimental observations. Although the extent of sp^3 hybridization may not mirror the experimental values, the trend itself is consistent with the experimental findings, marking a convergence between simulation with the EDIP potential and experiments [18]. It is interesting to note that the ReaxFF potential leads to a larger sp^3 to sp^2 fraction close to experiment (88% ReaxFF vs 98% experiment [18]) while the REBO potential gives such a fraction at 28%. Interestingly, with the EDIP and ReaxFF potentials, we could observe embedded nano-diamonds in the amorphous carbon phase in agreement with experiments using laser-induced transformations [39] as shown in SM Figure S5. It is interesting to note that your results are also in reasonable agreement with those of Ni et al [17] using a machine-learned C-C potential adjusted on DFT data: the structural evolution is found to follow the same order as found in this work i.e. molecular crystal → polymers → sp2 and sp3 hybrid carbon with crystal diamond and graphite depending on pressure.

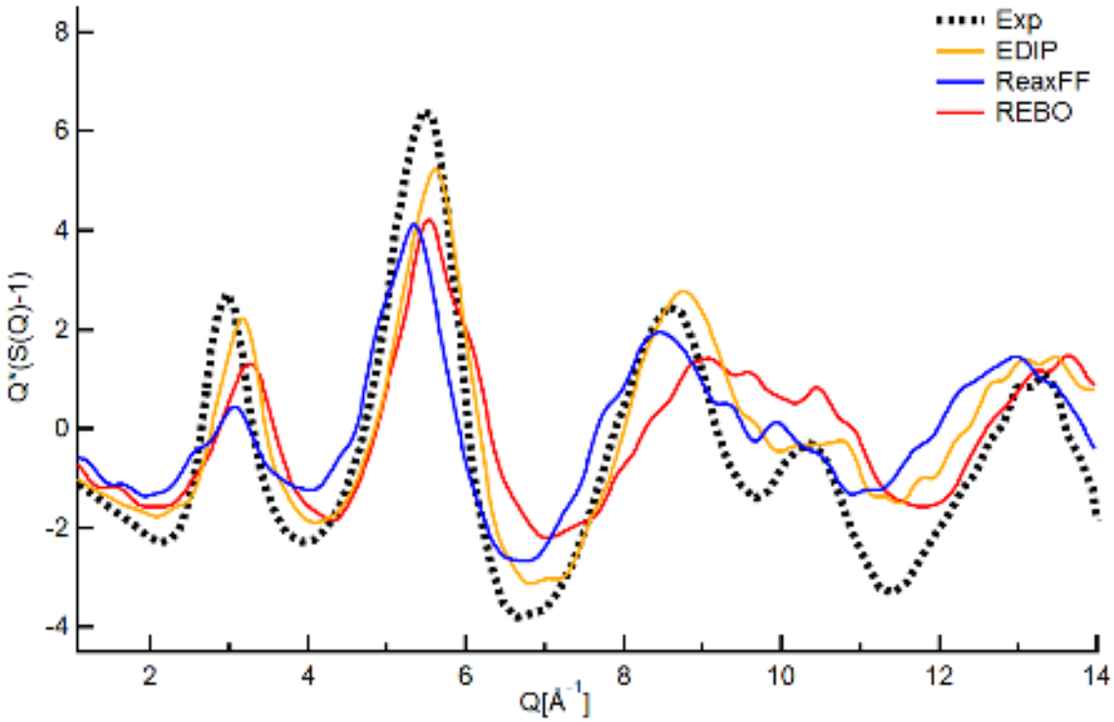

Figure 5: *Structure factor Q(S(Q) – 1) calculated at 60 GPa and 800 K with the REBO, EDIP and ReaxFF interatomic potentials, compared with experiment.*

We now turn to investigating the evolution of the system in terms of density, elastic modulus and sp^3 to sp^2 fraction (see Figures 5a,b,c) across the wide range of pressures (1 to 60 GPa) and temperatures (800 to 2000 K) considered in this work. For the sake of comparison, similar plots calculated with the REBO potential are given in SM Figure S4.

As shown in Figure 6a, with increasing pressure, the atoms within the C_{60} crystal come into closer proximity, resulting in a higher density. Interestingly, at lower pressures, an increase in temperature causes an increase in density (negative thermal expansion). However, at high pressures, the influence of temperature on density becomes less prominent, as pressure alone can significantly compress the system, rendering density primarily pressure-dependent. Figure 6b presents the variation of the bulk modulus of the FCC fullerene crystal. To evaluate the bulk modulus, we start by calculating the elastic constant matrix. When the system is at equilibrium, we calculate the pressure change induced by a variation in length along all components of the pressure tensor separately. The bulk modulus is calculated from this pressure tensor. At low pressure, the bulk modulus remains relatively stable with minimal temperature dependence. For instance, at 1 GPa and 800 K, where the system is molecular, the bulk modulus is below 200 GPa, increasing to 213 GPa after amorphization at 2000 K. A transition becomes evident at 2000 K, notably in the amorphous-layered phase change, resulting in a marked increase in bulk modulus. The layered phase exhibits a larger bulk modulus at a pressure of 30 GPa, reaching 443 GPa, while it approaches similar values at lower temperatures, such as 800 K. Subsequently, a pattern emerges where the bulk modulus peaks at 800 K before declining with increasing temperature until it rises again at 2000 K with the layer transition (it culminates at 800 K and 60 GPa). As the system remains amorphous across all temperatures from 60 GPa on, the bulk modulus tends to decrease with rising temperature.

When comparing these findings to experimental data, both similarities and differences emerge. Notably, the experiment reveals a peak bulk modulus at 27 GPa and 1273 K, exceeding 1000 GPa. In contrast, the simulations indicate that the peak bulk modulus is not attained until 60 GPa, at which point it reaches 990 GPa. However, simulations do show that the bulk modulus peaks at a specific temperature before diminishing as temperature further increases in qualitative agreement with experiments. It is interesting to note that compression simulations of Zhao et al [31] (that are not *stricto sensus* uniaxial) give stress values close to those found from our hydrostatic approach.

Figure 6c is a contour plot of the fraction of sp^3 bonds within different structural phases across varying temperatures and pressures. At low temperatures, specifically in the molecular and polymerized phases, the sp^3 fraction remains relatively low, staying below 15%. Between 20 and 40 GPa, the sp^3 fraction increases with temperature before declining again as layers form. Notably, layered configurations exhibit a lower sp^3 fraction compared to amorphous configurations. At 60 GPa, where layered configurations do not exist, the highest observed sp^3 fraction is obtained with amorphous carbon at 2000 K.

These observations tend to align with the experimental observation that amorphous carbon exhibits an increasing sp^3 fraction, reaching 65% sp^3 at 60 GPa. However, it's important to note that this fraction remains lower compared to achieving full sp^3 amorphous carbon, as observed in experiments. The disparity arises because, in the experimental data, the peak in the bulk modulus coincides with the peak sp^3 fraction. In contrast, our simulations indicate that at 60 GPa, the maximum bulk modulus is observed at 800 K, while the peak sp^3 fraction is observed at 2000 K.

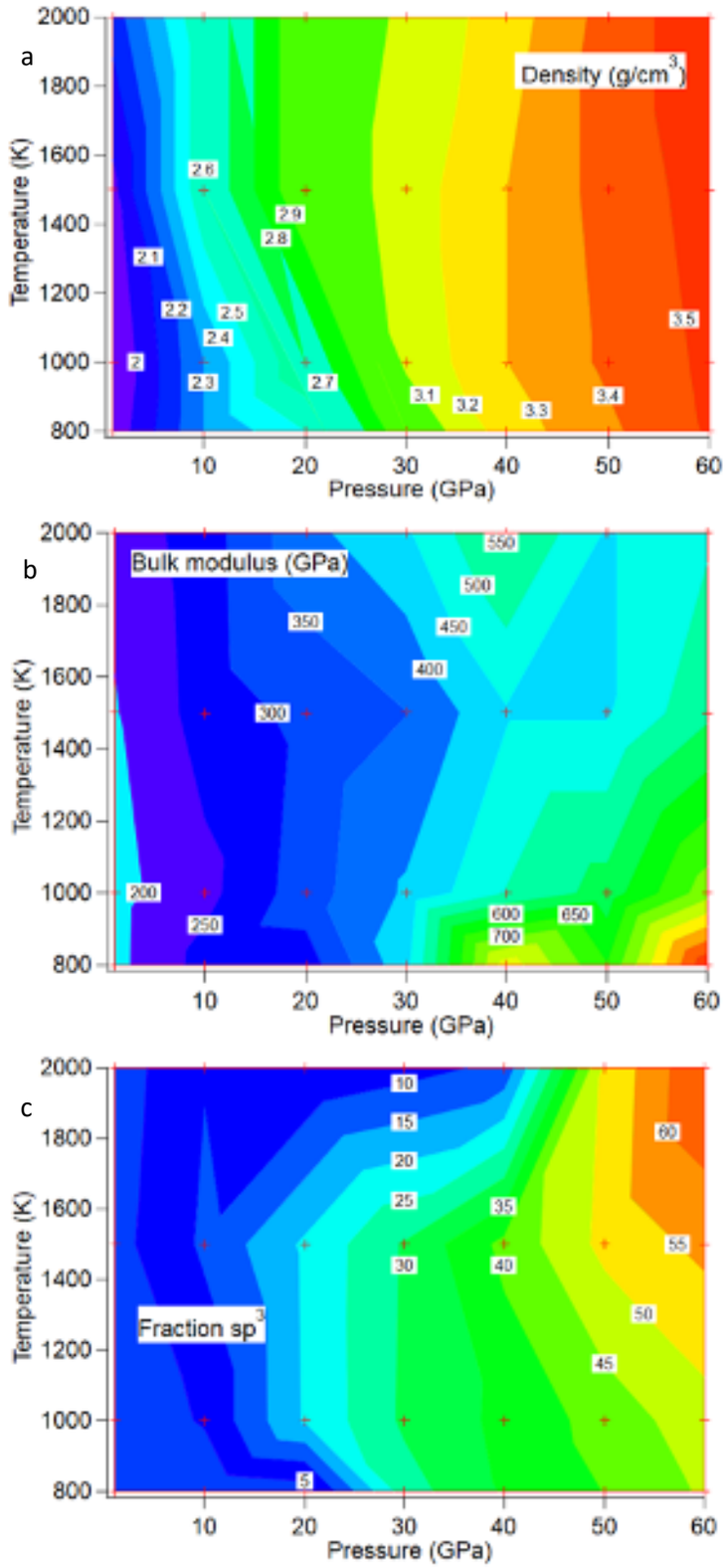

Figure 6: *Contour plots for (a) density, (b) bulk modulus and (c) sp^3/sp^2 fraction (in percent), as a function of Pressure and Temperature, calculated with the EDIP potential. See SM, Table S1*

Conclusion

Our in-depth study focused on the phase changes of FCC C_{60} crystals under pressure and temperature using MD simulations and different interatomic C-C reactive potentials. All three potentials agree, at least qualitatively, with experiments in terms of the ability to stabilize the different phases (C_{60} molecular crystal, polymerized C_{60}, amorphous carbon) within reasonable (P, T) ranges. We note, however, that a layered structure is positively identified only with EDIP, whereas this phase might require a longer time scale and higher temperatures to appear with REBO and ReaxFF.

This study demonstrates that the EDIP C-C potential is superior to REBO and ReaxFF when it comes to very high temperature and pressure transformations regarding the presence of nano-diamonds embedded in an amorphous carbon phase and final transformation into a defective graphite-like layered texture. We concentrated our effort on simulations based on the EDIP C-C potential acknowledging that ReaxFF performs well in milder P,T conditions.

At low pressure and low temperature conditions, the C_{60} crystal retains its molecular state, characterized by a positive thermal expansion as temperature rises. However, as pressure and temperature are incrementally increased, a transition occurs, leading to the formation of a polymerized system. This polymerized system exhibits negative thermal expansion. Under the influence of high temperature and under 40 GPa, the system undergoes a further transformation into an amorphous carbon system and/or a layered defective graphite-like system. Furthermore, despite some differences in the simulation conditions compared to those in the recent experiments of Zhang *et al.* [18], we obtain similar observations and results regarding phase's structure factor and bulk modulus. However, it's important to note that the calculated sp^3 fraction (at most 65%) is generally lower than the observed experimental value (90%). This feature, common to all considered interatomic reactive potentials, reflects the difficulty in modelling sp2 C-C bonds to into sp3's transformation kinetics although ReaxFF does reproduce well accurate DFT energy barrier calculations (see SM Figure S3). Our findings can be summarized as shown in Table 1:

Temperature and Pressure range: T [800 -2500 K], P [1- 60 GPa]					
	C_{60} molecular crystal	**C_{60} polymerized**	**Amorphous carbon (AC)**	**Nanodiamonds in AC**	**Graphite / layered texture**
REBO	Not in this P range	Yes	Yes	Not good re sp^3 fraction	Some trends, but no clear evidence
EDIP	Yes	Yes	Yes	Yes	Yes
ReaxFF	Yes	Yes	Yes	Yes but longer trajectories are needed	Yes

Table 1: *Summary of our evaluation of REBO, EDIP and ReaxFF potentials. "Yes" means a correct qualitative agreement with experiment.*

Our high-pressure, high-temperature simulation study provides valuable qualitative insights on the fate of a pristine C_{60} molecular crystal under extreme conditions in qualitative agreement with experiments. Having identified their strengths and weaknesses enables using EDIP and ReaxFF in situations where a reasonably fast and accurate C-C interatomic potential should be used, for example to model the structure of carbon incorporated in the porosity of cement.

Supplementary Material

The Supplementary Material section contains additional information regarding pair distribution functions for the various interatomic potentials considered in this work including a detailed analysis of their various contributions in terms of rank 1-4 neighbors. The energy barriers relative to the transition from Rhombohedral graphite to diamond is provided for the first time to our knowledge using the REBO, EDIP and ReaxFF potentials and compared to DFT calculations. Additional ReaxFF simulations in conditions reported for liquid C60 showing actual polymerization. Additional {A, P, T} contour plots are also provided for the REBO potential where A= density, bulk modulus and fraction of sp3 bonds.

Acknowledgment

KH wishes to thank CNRS for his “International PhD” fellowship.

References

[1] H. W. Kroto, J. R. Heath, S. C. O'Brien, R. F. Curl, and R. E. Smalley, "C60: Buckminsterfullerene", *Nature*, vol. 318, no. 6042, pp. 162–163, Nov. 1985, doi: 10.1038/318162a0.

[2] Z. Du, N. Jannatun, D. Yu, J. Ren, W. Huang, and X. Lu, "C60-Decorated nickel-cobalt phosphide as an efficient and robust electrocatalyst for hydrogen evolution reaction", *Nanoscale*, vol. 10, no. 48, pp. 23070–23079, Dec. 2018, doi: 10.1039/c8nr07472k.

[3] B. Wang *et al.*, "Tuning electron transfer in supramolecular nano-architectures made of fullerenes and porphyrins", *Nanoscale*, vol. 11, no. 22, pp. 10782–10790, Jun. 2019, doi: 10.1039/c9nr02824b.

[4] A. A. Arie, W. Chang, and J. K. Lee, "Effect of fullerene coating on silicon thin film anodes for lithium rechargeable batteries", *Journal of Solid State Electrochemistry*, vol. 14, no. 1, pp. 51–56, Jan. 2010, doi: 10.1007/s10008-009-0787-4.

[5] N. MacKiewicz *et al.*, "Fullerene-functionalized carbon nanotubes as improved optical limiting devices", *Carbon N Y*, vol. 49, no. 12, pp. 3998–4003, 2011, doi: 10.1016/j.carbon.2011.05.040.

[6] M. Álvarez-Murga and J. L. Hodeau, "Structural phase transitions of C60 under high-pressure and high-temperature", *Carbon N Y*, vol. 82, no. C, pp. 381–407, 2015, doi: 10.1016/j.carbon.2014.10.083.

[7] S. J. Duclos, K. Brister, R. C. Haddon, A. R. Kortan, and F. A. Thiel, "Effects of pressure and stress on C60 fullerite to 20 GPa", *Nature*, vol. 351, no. 6325, pp. 380–382, May 1991, doi: 10.1038/351380a0.

[8] F. Moshary *et al.*, "Gap reduction and the collapse of solid C60 to a new phase of carbon under pressure", *Phys Rev Lett*, vol. 69, no. 3, pp. 466–469, Jul. 1992, doi: 10.1103/PhysRevLett.69.466.

[9] V. Blank *et al.*, "Is C60 fullerite harder than diamond?", *Phys Lett A*, vol. 188, no. 3, pp. 281–286, May 1994, doi: 10.1016/0375-9601(94)90451-0.

[10] R. S. Ruoff and A. L. Ruoff, "Is C60 stiffer than diamond?", *Nature*, vol. 350, no. 6320, pp. 663–664, Apr. 1991, doi: 10.1038/350663b0.

[11] Y. Iwasa *et al.*, "Pressure-induced cross-linking of C60", *Synth Met*, vol. 70, no. 1–3, pp. 1407–1408, Mar. 1995, doi: 10.1016/0379-6779(94)02898-9.

[12] V. D. Blank *et al.*, "Ultrahard and superhard carbon phases produced from C60 by heating at high pressure: structural and Raman studies", *Phys Lett A*, vol. 205, no. 2–3, pp. 208–216, Sep. 1995, doi: 10.1016/0375-9601(95)00564-J.

[13] D. S. Sabirov, O. Ori, A. A. Tukhbatullina, and I. S. Shepelevich, "Covalently bonded fullerene nano-aggregates (C60)n: Digitalizing their energy–topology–symmetry", *Symmetry (Basel)*, vol. 13, no. 10, Oct. 2021, doi: 10.3390/sym13101899.

[14] E. Meirzadeh *et al.*, "A few-layer covalent network of fullerenes", *Nature*, vol. 613, no. 7942, pp. 71–76, Jan. 2023, doi: 10.1038/s41586-022-05401-w.

[15] B. Sundqvist, "Buckyballs under pressure", *Phys Status Solidi B Basic Res*, vol. 223, no. 2, pp. 469–477, Jan. 2001, doi: 10.1002/1521-3951(200101)223:2<469::AID-PSSB469>3.0.CO;2-2.

[16] B. Sundqvist, "Polymeric Fullerene Phases Formed Under Pressure", in *Fullerene-Based Materials: Structures and Properties*, 2004, pp. 85–126. doi: 10.1007/b94380.

[17] K. Ni, F. Pan, and Y. Zhu, "Structural Evolution of C60 Molecular Crystal Predicted by Neural Network Potential", *Adv Funct Mater*, vol. 32, no. 42, Oct. 2022, doi: 10.1002/adfm.202203894.

[18] Y. Shang *et al.*, "Ultrahard bulk amorphous carbon from collapsed fullerene", *Nature*, vol. 599, no. 7886, pp. 599–604, Nov. 2021, doi: 10.1038/s41586-021-03882-9.

[19] M. Moseler, H. Riedel, P. Gumbsch, J. Stäring, and B. Mehlig, "Understanding of the phase transformation from fullerite to amorphous carbon at the microscopic level", *Phys Rev Lett*, vol. 94, no. 16, Apr. 2005, doi: 10.1103/PhysRevLett.94.165503.

[20] A. P. Thompson *et al.*, "LAMMPS - a flexible simulation tool for particle-based materials modeling at the atomic, meso, and continuum scales", *Comput Phys Commun*, vol. 271, p. 108171, Feb. 2022, doi: 10.1016/j.cpc.2021.108171.

[21] G. J. Martyna, D. J. Tobias, and M. L. Klein, "Constant pressure molecular dynamics algorithms", *J Chem Phys*, vol. 101, no. 5, pp. 4177–4189, Sep. 1994, doi: 10.1063/1.467468.

[22] N. R. Tummala, C. Bruner, C. Risko, J. L. Brédas, and R. H. Dauskardt, "Molecular-scale understanding of cohesion and fracture in P3HT: Fullerene blends", *ACS Appl Mater Interfaces*, vol. 7, no. 18, pp. 9957–9964, May 2015, doi: 10.1021/acsami.5b02202.

[23] N. A. Marks, "Generalizing the environment-dependent interaction potential for carbon", *Phys Rev B Condens Matter Mater Phys*, vol. 63, no. 3, Dec. 2001, doi: 10.1103/PhysRevB.63.035401.

[24] C. de Tomas, I. Suarez-Martinez, and N. A. Marks, "Graphitization of amorphous carbons: A comparative study of interatomic potentials", *Carbon N Y*, vol. 109, pp. 681–693, Nov. 2016, doi: 10.1016/j.carbon.2016.08.024.

[25] K. Chenoweth, A. C. T. van Duin, and W. A. Goddard, "ReaxFF Reactive Force Field for Molecular Dynamics Simulations of Hydrocarbon Oxidation", *J Phys Chem A*, vol. 112, no. 5, pp. 1040–1053, Feb. 2008, doi: 10.1021/jp709896w.

[26] L. Pintschovius, O. Blaschko, G. Krexner, and N. Pyka, "Bulk modulus of C60 studied by single-crystal neutron diffraction", *Phys Rev B*, vol. 59, no. 16, pp. 11020–11026, Apr. 1999, doi: 10.1103/PhysRevB.59.11020.

[27] B. Sundqvist, "Carbon under pressure", *Physics Reports*, vol. 909. Elsevier B.V., pp. 1–73, May 08, 2021. doi: 10.1016/j.physrep.2020.12.007.

[28] V. D. Blank, S. G. Buga, G. A. Dubitsky, N. R. Serebryanaya, M. Yu. Popov, and B. Sundqvist, "High-pressure polymerized phases of C 60", *Carbon N Y*, vol. 36, no. 4, pp. 319–343, 1998, doi: 10.1016/S0008-6223(97)00234-0.

[29] A. C. T. Van Duin, S. Dasgupta, F. Lorant, and W. A. Goddard, "ReaxFF: A reactive force field for hydrocarbons", *Journal of Physical Chemistry A*, vol. 105, no. 41, pp. 9396–9409, Oct. 2001, doi: 10.1021/jp004368u.

[30] J. Laranjeira and L. Marques, "C60 structures: Structural, electronic and elastic properties", *Mater Today Commun*, vol. 23, Jun. 2020, doi: 10.1016/j.mtcomm.2020.100906.

[31] Y. Zhao, C. Qian, V. Gladkikh, and F. Ding, "Simulated Pressure-temperature Carbon Structure Map obtained through uniaxial compression of Bulk C60", *Carbon N Y*, vol. 202, pp. 554–560, Jan. 2023, doi: 10.1016/j.carbon.2022.11.007.

[32] J. Leyssale, B. Farbos, J. Da Costa, P. Weisbecker, G. Chollon, and G. L. Vignoles, "Analysis and molecular modeling of pyrolytic carbons nanotextures", Ceram. Trans. 248., 2014, pp. 45–53. doi: 10.1002/9781118932995.ch6.

[33] D. Costa, G. Pellicane, C. Caccamo, E. Schöll-Paschinger, G. Kahl, " Theoretical description of phase coexistence in model C60", Physical Review E - Statistical, Nonlinear, and Soft Matter Physics, 68(2 1). https://doi.org/10.1103/physreve.68.021104]

[34] C. Bichara, J.-Y. Raty, and J.-P. Gaspard, "Structure and bonding in liquid tellurium", *Phys Rev B*, vol. 53, no. 1, pp. 206–211, Jan. 1996, doi: 10.1103/PhysRevB.53.206.

[35] S. Fahy, S. G. Louie, and M. L. Cohen, "Theoretical total-energy study of the transformation of graphite into hexagonal diamond", *Phys Rev B*, vol. 35, no. 14, pp. 7623–7626, May 1987, doi: 10.1103/PhysRevB.35.7623.

[36] J. M. Soler *et al.*, "The SIESTA method for ab initio order- N materials simulation", *Journal of Physics: Condensed Matter*, vol. 14, no. 11, pp. 2745–2779, Mar. 2002, doi: 10.1088/0953-8984/14/11/302.

[37] E. Artacho *et al.*, "The SIESTA method; developments and applicability", *Journal of Physics: Condensed Matter*, vol. 20, no. 6, p. 064208, Feb. 2008, doi: 10.1088/0953-8984/20/6/064208.

[38] E. Artacho, D. Sánchez-Portal, P. Ordejón, A. García, and J. M. Soler, "Linear-Scaling ab-initio Calculations for Large and Complex Systems", *Physica Status Solidi (b)*, vol. 215, no. 1, pp. 809–817, Sep. 1999, doi: 10.1002/(SICI)1521-3951(199909)215:1<809::AID-PSSB809>3.0.CO;2-0.

[39] H. Tian, Z. Yao, Z. Li, J. Guo, and L. Liu, "Unlocking More Potentials in Two-Dimensional Space: Disorder Engineering in Two-Dimensional Amorphous Carbon", *ACS Nano*. American Chemical Society, 2023. doi: 10.1021/acsnano.3c09593.